ABSTRACT

Title: COMPARISON OF ADVANCED RESIST ETCHING IN E-BEAM GENERATED PLASMAS

Bryan J. Orf, Masters of Science, 2006

Directed By: Professor Gottlieb S. Oehrlein, Department of Material Science and Engineering and Institute for Research in Electronics and Applied Physics

The use of e-beam based plasma as a source for plasma-polymer interactions was investigated employing two advanced photoresists that differed significantly in polymer structure. The influence of Ar^+ bombardment energy, chemically-assisted etching using fluorine, and the effects of the presence of a thin fluorocarbon (FC) layer on surface roughness evolution and etching rates of the blanket photoresists were determined. Low energy ion bombardment increased surface roughness. Small amounts of fluorine (5% SF_6/Ar), resulted in a further increase of the surface roughness and etch rate over values of Ar^+ ion bombardment alone. An unexpected result was that the photoresist surface roughness evolved during the afterglow of an Ar plasma and decreased for long afterglows (300 ms). It was shown that the roughness of an FC overlayer impact the photoresist underlayer etching and surface roughening. The magnitude of the change was dependent on the conditions under which the FC overlayer is deposited.

COMPARISON OF ADVANCED RESIST ETCHING IN E-BEAM GENERATED PLASMAS

By

Bryan J. Orf

Thesis submitted to the Faculty of the Graduate School of the
University of Maryland, College Park, in partial fulfillment
of the requirements for the degree of
Master of Science
2006

Advisory Committee:
Professor Gottlieb Oehrlein, Chair
Professor John Melngailis
Dr. Darrin Leonhardt

© Copyright by
Bryan J. Orf
2006

Acknowledgements

I would like to acknowledge Professor Oehrlein for his assistance and guidance throughout this process. His honesty, discussions, direction and ideas were crucial for this thesis. I would like to thank you for helping develop my research and data analysis abilities. I am also thankful for providing us with facilities that are unique in the field of our research and great opportunities to interact with scientists in academia and industry.

Additionally, I would like to thank Dr. Leonhardt and Dr. Walton for your support and guidance, through all the trials and tribulations, as well as the great opportunity to work with all of the state of the are equipment as well as all of the novel ideas, and discussions.

I would be remiss if I didn’t also acknowledge my various research financial supports: Office of Naval Research, Lam Research Corporation, Texas Instruments and the National Science Foundation under award No. DMR-0406120.

I would like to thank my colleagues, Sebastian Engelmann, Li Ling, XueFeng Hua, Ming-shu Kuo, and Robert Bruce for helpful discussion and assistance in the work presented in this thesis and in the maintenance of the lab and equipment.

I am grateful to the members of my dissertation committee for reading my thesis. Thank you Professor Melngailis and Dr. Leonhardt.

Finally I would like to thank my family. Without your love and support I would not have made it through my studies. Mom and Dad, I will always be grateful for the unwavering support you have given me.

Table of Contents

Acknowledgements ii
Table of Contents iii
List of Tables iv
List of Figures v
Chapter 1: Introduction 1
1.1 Plasma Processing of Advanced Materials (Polymers/Photoresists) 1
1.2 Introduction to Various Plasma Sources 2
1.2.1 ICP 3
1.2.2 CCP 3
1.2.3 LAPPS (E-Beam) 4
1.2.4 Increasing Ion Energy to Surfaces 6
1.3 Current Work 6
1.4 Outline of Thesis 7
Chapter 2: Study of Photoresist Etching and Roughness Formation in Electron-Beam Generated Plasmas 8
2.1 Introduction 10
2.2 Experimental setup and procedure 11
2.2.1 Photoresists 11
2.2.2 LAPPS 11
2.2.3 Ex Situ Analysis 13
2.2.4 Thin FC Layer 14
2.3 Results 14
2.3.1 Effect of Fluorine Addition 16
2.3.2 Thin FC layer 18
2.4 Discussion 21
2.5 Conclusions 23
Chapter 3: Temporal Behavior and Fluence Changes in LAPPS during Photoresist Etching 24
3.1 Introduction 24
3.2 Experimental Setup 24
3.2.1 Photoresists 25
3.2.2 Argon Experiments (SS chamber) 25
3.3 Results 26
3.4 Discussion 32
3.4.1 Effect of Pulsed LAPPS 33
3.4.2 Ar^+ Ion Bombardment 35
3.4.3 Fluence 36
3.5 Conclusions 38
Chapter 4: General Conclusions 39
References: 41

List of Tables

Table 1.1: Plasma and sample characterization tools used for this work. 7

Table 3.1: Calculated etch yield and RMS roughness as a function of fluence for various conditions. 37

List of Figures

Figure 1.1 Schematic of LAPPS plasma reactor used in this work 5

Figure 2.1 Chemical Structure of 193 and 248 nm photoresist polymers. 11

Figure 2.2 Schematic diagram of LAPPS. a) cross sectional detail of linear hollow cathode construction b) schematic of etching chamber 13

Figure 2.3 a) Etch rate as a function of RF bias in pure Ar and 5% SF_6/Ar electron-beam generated plasmas. b) RMS roughness at varying bias voltages for Ar and 5%SF_6/Ar plasmas. Virgin photoresist RMS roughness are shown for the 193 and 248 nm PR. The pressure was 95 mTorr for all SF_6 experiments and the pressure for Ar changes from 24 to 25 to 27.5 mTorr with increasing bias voltage which gave the same ion currents at the wafer stage. All other experimental parameters were at standard conditions. 15

Figure 2.4 a) The 193 nm and 248 nm photoresist etch rates at varying percentage of SF_6 in Ar plasma. b) The RMS roughness at varying percentage SF_6. The samples were run at equivalent ion currents and a 10V applied bias. 16

Figure 2.5 The RMS roughness per nm PR etched versus RF bias voltage. The samples were run at standard conditions expect for the applied bias. The operating pressure for the pure Ar plasmas were 24 to 25 to 27.5 mTorr with increasing bias voltage, and the 5%SF6/Ar plasmas were run at 95 mTorr to keep the ion currents the same for different experiments. 17

Figure 2.6 a)5% SF6/Ar plasmas showing the effect on etch depth per pulse and b) RMS roughness of varying pulse afterglow times for T_{on} = 4 ms. Experiments were performed at otherwise standard conditions with a 10 V applied bias. 18

Figure 2.7 AFM images of blanket FC films deposited on 193 nm photoresist before and after Ar etching. (a) C_4F_8/90%Ar FC deposiion (b) C_4F_8 FC deposition. Pre and post Ar plasma LAPPS exposures at 50 V RF bias are shown for both situations. 19

Figure 2.8 a) RMS and PR etch rate of C_4F_8 deposited FC layer/PR in an Ar plasma as a function of FC film thickness for 248 nm PR's b)Same for C_4F_8 deposited FC layer/193 nm PR stacks. The experiments were run at standard conditions using pure Ar. 20

Figure 2.9 a) RMS and PR etching depth of a C_4F_8/90%Ar FC layer/248 nm PR stack in an Ar LAPPS plasma as a function FC thickness. b) Same for C_4F_8/90%Ar deposited FC layer/193 nm PR stacks. The experiments were run at standard conditions using pure Ar. 21

Figure 3.1 Chemical Structures of 193 and 248 nm photoresist materials. 25

Figure 3.2 Schematic diagram of LAPPS set up used for the temporal experiments (Stainless Steel chamber). 26

Figure 3.3 Schematic of LAPPS operation showing the voltage and etch rate vs time. 27

Figure 3.4 Standard analysis of photoresist etching: temporal dependencies. 28

Figure 3.5 193 nm PR plots of etch depth per pulse as a function of T_{on} and T_{off}. Processing done in the SS chamber with a 10 V bias and a pure Ar discharge. 29

Figure 3.6 193 nm PR plots of RMS roughness per pulse as a function of T_{on} and T_{off}. Processing was done in the SS chamber with a 10 V applied bias and a pure Ar discharge. 30

Figure 3.7 193 nm PR etch rate as a function of Ton. Processing was done in the SS chamber with a 10V applied bias, T_{off} of 300 ms, and in a pure Ar discharge. 31

Figure 3.8 193 nm PR plots of RMS roughness and etch rate as a function of bias. Processing done in the SS chamber with a total run time of 25 min and in a pure Ar discharge. The RMS roughness corresponding to ~0.33 is the unexposed PR roughness. 32

Chapter 1: Introduction

1.1 Plasma Processing of Advanced Materials (Polymers/Photoresists)

The science underlying the design of microcircuits rests on solid state physics, but, to an increasing extent, the fabrication of microcircuits relies on the physics and chemistry of plasmas. Plasma etching and deposition processes are indispensable in many semiconductor manufacturing steps, and are better than wet-chemistry alternatives for others. As circuit size continues to decrease, the low-density plasmas used in chip-making have been replaced by high-density plasmas. These plasmas involve new phenomena and require more sophisticated simulation and analysis.

Plasma processes are desirable in microelectronics production, largely because plasmas can produce anisotropic etching and deposition, while wet chemistry tends to produce more damaging isotropic processes. Fabrication of microcircuits requires several cycles of layer deposition as well as the etching of these layers. Plasma etching typically requires etchant-resistant photoresists to protect portions of the underlying layers. Photoresists are “patterned” optically by exposing them to (UV) radiation shone through a mask.

In plasmas, the potential that accelerates the ions to the surface is generated by the plasma sheath. The sheath is formed because the electrons are more mobile than the ions, due to their smaller mass. As fast-moving electrons leave the plasma more rapidly than the ions, the plasma develops a positive potential with respect to its surroundings. Thus ions are accelerated when they leave the plasma. This extra ion energy allows surface chemical reactions that could not otherwise take place for lack of energy.

The problem with current plasma etching processes is that the etchants can roughen the photoresist, making the resultant pattern different than intended. In addition, in conventional etchers (capacitive-coupling devices), the input power determines both the ion flux and the accelerating potential. The inability to independently control these two variables poses a problem. Too high an accelerating potential can damage thin wafer layers while lowering the ion flux slows the process.

Chemical reactions generated by the plasma during etching or deposition can be complex, as they involve neutral species, ions, and free radicals. For those designing the plasma-processing devices and controlling their parameters, a key goal is uniformity of etch rate and assurance of correct etching across the entire wafer. Ion energy controlled directly by the bias voltage at the wafer is a good "control knob" for etch rates. However, radial uniformity can be sensitive to power input location, wall material, temperature, and other variables.

With these challenges in mind, this thesis describes the results of our research on etch and surface roughening mechanisms of two photoresists and plasma-polymer reactions in a high density electron beam based plasma system.

1.2 Introduction to Various Plasma Sources

In the following paragraphs, a brief review of the basic aspects of inductively coupled, capacitively coupled, and electron beam (e-beam) based plasma sources are presented. The e-beam reactor was used in this research because of its distinct advantages for studying plasma-polymer (photoresist) reactions.

1.2.1 ICP

An inductively coupled plasma (ICP) is a type of plasma source in which the energy is supplied by electrical currents that are produced by electromagnetic induction, that is, by time-varying magnetic fields [1.1-1.7]. There are two types of ICP geometries: planar and cylindrical. In planar geometry, the electrode is a coil wound into a flat spiral. In cylindrical geometry, the electrode is helical, like a spring. A radio-frequency (RF) voltage applied to the coil creates a varying magnetic field around it, which induces an electric current in the gas, leading free electrons to break down and form a plasma. ICP discharges are of relatively high electron density, up to $n_p \approx 10^{13}$ cm^{-3}. As a result, ICP discharges have wide applications where a high density plasma is necessary. Another benefit of ICP discharges is that they are relatively free of contamination because the electrodes can be completely outside the reaction chamber. Some drawbacks of ICP reactors are that they require coupling windows and possess a small capacitive coupling component (leading to window erosion and plasma contamination), high RF plasma potential affects the minimal ion energy, and they have a high cost for RF power sources and matching devices, especially when scaled to large areas.

1.2.2 CCP

A CCP is one of the most common types of industrial plasma reactors because of its simplicity. It consists of two metal electrodes separated by a small distance (a few cm) [1.8-1.12]. One of these two electrodes is connected to an RF power supply and is typically driven from 100-2000 W, while the other electrode is grounded. (In the case of a 'dual frequency' CCP, the second electrode is driven at a lower frequency to help control the energies of ions bombarding the substrate). As this configuration is similar in principle to

a capacitor in an electric circuit, the plasma is called a capacitively coupled plasma. When the RF electric field is applied to the powered electrode, the free electrons in the gas respond and are accelerated (acquire energy). The heated electrons collide with gas molecules until "breakdown" is reached, where the gas has become sufficiently ionized by the hot electrons. After breakdown, the plasma is formed and becomes electrically conductive. Typically plasma densities of capacitively coupled plasma are relatively low in the range of $n_p \approx 10^9$-10^{11} cm^{-3}. The pressure used in capacitively coupled plasma reactors is typically in the range of 20-300 mTorr, and is usually higher than that used in inductively coupled high-density plasma reactors. CCP's hold advantages over ICPs because etching selectivity of materials relative to photoresist is poor in inductively coupled plasma sources. In contrast with ICP, the electrodes are placed inside the reactor and are thus exposed to the plasma and subsequent reactive chemical species. The plasma potential and the floating potential can be very high in capacitively coupled plasma reactors, ranging from tens to hundreds of volts.

1.2.3 LAPPS (E-Beam)

The Naval Research Laboratory (NRL) developed a plasma-based materials processing tool utilizing electron beam (e-beam) generated plasmas (Fig 1.1) [1.13]. Unlike conventional plasma sources used in materials processing applications that apply external [electromagnetic] fields to breakdown gases, e-beam ionization produces a plasma that is independent of the chamber layout and is readily scalable. Furthermore, since the plasma electrons are not being heated by external fields to sustain the plasma, the plasmas possess low electron temperatures and internal fields, resulting in low ion energies. It has been shown that the Large Area Plasma Processing System (LAPPS) is an inherently

scalable system with a large surface-to-volume ratio plasma [1.14-1.16]. The plasma production is decoupled from stages, system geometry, and materials. This is in conjunction with producing high density ($n_p \approx 10^{11}$-10^{12} cm^{-3}) plasmas with low electron temperatures (≤ 0.5 eV), allowing unprecedented process control and a plasma density variable with e-beam current. The ion and radical production is directly proportional to the gas composition. Fluxes to the surface can be varied with distance from the e-beam ionization region. Ion energies arriving at surfaces are < 5 eV, which can be raised with electrode biasing. LAPPS' advantages include the independent control of ion and free radical fluxes to the surface, very high uniformity, low ion energies that were previously unattainable and a geometry that is well suited for many applications.

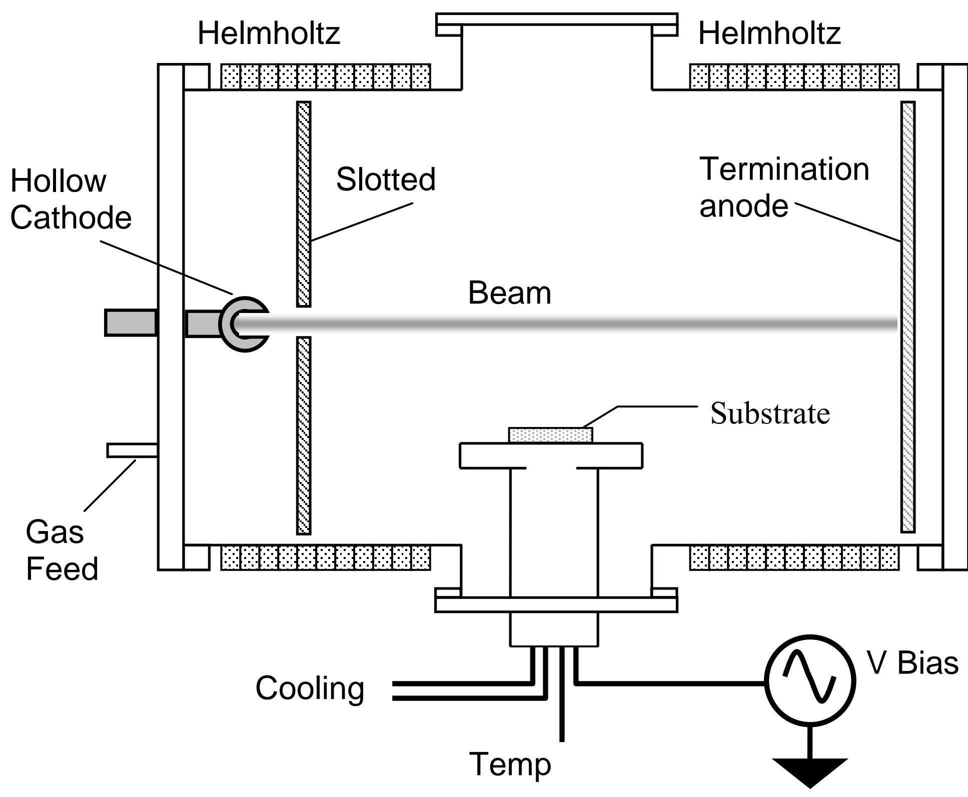

Figure 1.1 Schematic of LAPPS plasma reactor used in this work

1.2.4 Increasing Ion energy to Surfaces

In many applications, it is necessary to increase the energy of the ions to the substrate to increase the etching rate. This was done in LAPPS by applying an RF bias to the processing stage. The front electrode of the stage was electrically isolated from the stage body so that an RF-induced negative DC bias (bias voltage) could be applied to the substrate to vary the incident ion energies during the plasma pulse. RF power was applied to the stage through a commercial matchbox (RFPP Model AM-5) by an RF amplifier/signal generator operating at 13.56 MHz. The RF power was only applied during the e-beam pulse. The 'bias' mentioned in the forthcoming sections is the negative DC offset voltage that was measured, not the positive value quoted.

1.3 Current Work

In order to provide a comprehensive characterization of plasma properties, a variety of complementary measurements were taken to obtain information about etching and surface evolution. After plasma modification, the sample was characterized by atomic force microscopy (AFM) and ellipsometry. Our studies involved collaborative efforts between the NRL and the University of Maryland (UMD). A summary of the measurements involved in this thesis and the contributions of each laboratory are shown in Table 1.1.

Measurement	**Method**	**Location**	**Information**
Ellipsometry	*Ex situ*	UMD	Etch/deposition rates, optical properties
Atomic force microscopy	*Ex situ*	NRL	Surface morphology
LAPPS		NRL	E-beam based plasma system
DF-CCP		UMD	Dual Frequency Capacitively Coupled Plasma System

Table 1.1: *Plasma and sample characterization tools used for this work.*

1.4 Outline of Thesis

This thesis summarizes the results of plasma-polymer interactions in the LAPPS system and the studies on plasma etching and surface roughening of advanced electronic materials.

Plasma-based pattern transfer of lithographically produced nanoscale patterns in advanced photoresist materials is often accompanied by photoresist surface roughening and line edge roughening due to factors that are not well understood. In Chapter 2, the evolution of surface roughening and etching in 193 nm and 248 nm photoresist materials during plasma processing as a function of plasma operating parameters is presented. In the CCP, a small gap structure placed over the sample provided a region that shadowed ion bombardment. The gap structure was also used to deposit a thin fluorocarbon layer on the substrates to simulate how a fluorocarbon gas reacts in LAPPS. In Chapter 3 the temporal dependency on the etch rate and RMS roughness of LAPPS on two novel photoresists are presented. The changes between two chambers, and the effect of a high and low fluence are also shown. Finally, Chapter 4 summarizes the main conclusions of this Masters thesis.

Chapter 2: STUDY OF PHOTORESIST ETCHING AND ROUGHNESS FORMATION IN ELECTRON-BEAM GENERATED PLASMAS

Bryan J. Orf
Department of Materials Science and Engineering and Institute for Research in Electronics and Applied Physics, University of Maryland College Park, MD 20742

Darrin Leonhardt, Scott G. Walton
Plasma Physics Division, U.S. Naval Research Laboratory Washington, DC 20375-5346

Gottlieb S. Oehrlein
Department of Materials Science and Engineering and Institute for Research in Electronics and Applied Physics, University of Maryland College Park, MD 20742

Abstract:

A modulated electron beam generated plasma processing system was used to study plasma-polymer interactions for two photoresists that differed significantly in polymer structure. The two photoresists (PR) used were a 193 nm photoresist material based on a methacrylate main chain containing lactone and adamantane based functional groups and a 248 nm photoresist based on an aromatic polymer. Because of the low plasma potential of the electron-beam generated plasma, we were able to study plasma etching and surface roughening of the photoresists at very low ion energies. The effects of Ar^+ ion bombardment energy, influence of chemically-assisted etching using fluorine employing SF_6/Ar, and the presence of a thin fluorocarbon (FC) overlayer on photoresist etching surface roughness formation were examined. The plasma discharges were pulsed. Typical conditions in the experiments were 4 ms pulses (T_{on}), 20 ms period (16 ms T_{off}) by a 2 kV pulsed e-beam generated plasma with a 50 sccm total gas flow rate. RF biasing producing a dc bias of up to 50 V was applied to the processing stage. The

pressure for different gas chemistries was selected to give the same ion currents at the stage and was in the range 24 to 95 mTorr. Small amounts of fluorine (5% SF_6/Ar), resulted in higher PR etching rates and an increased surface roughness relative to values measured for Ar discharges. At a 50 V bias the etch rate was ~ 2 times greater for the SF_6 based plasma than for a pure Ar. Typical RMS roughness for an Ar plasma up to 50 V RF bias range up to 0.4 nm. The addition of SF_6 increased the overall RMS roughness in all cases, e.g. to 0.65 nm at 50 V RF bias. Even though there is greater overall roughness for a SF_6/Ar plasma than for a pure Ar discharges, the RMS roughness per nm of photoresist removed is greater for pure Ar discharges than for the SF_6/Ar mixtures. We also observed that the 248 nm photoresist shows less surface roughness than 193 nm photoresist after identical treatments, which is explained by a higher etching rate of the 193 nm photoresist material since the RMS roughness per nm photoresist etched is greater for 248 nm photoresist material than for 193 nm photoresist (at 10 V bias). The roughness of a thin FC overlayer is transferred in an Ar discharge into the photoresist underlayer, but for thick FC overlayers the etched PR surface is smoother than the initial FC overlayer roughness.

2.1. Introduction:

Plasma modification of polymer surfaces has been widely applied in materials research [2.1-2.5]. Plasmas can be used to tailor surface energy and reactivity of polymeric materials without interfering with the bulk polymer properties. Input power, pressure, degree of ionization and other plasma parameters all affect the outcome of plasma-polymer interactions [2.6-2.9]. The Naval Research Laboratory (NRL) has developed a plasma processing tool called LAPPS (Large Area Plasma Processing System) that utilizes a pulsed electron beam (e-beam) for plasma generation. We have applied LAPPS in an effort to shed light on the surface roughening problem seen in the processing of 193 nm photoresist materials, and performed comparative etching studies using a 193 nm PR material and a 248 nm PR material. The 193 nm photoresist material is based on a methacrylate main chain containing lactone and adamantane based functional groups and the 248 nm photoresist is based on an aromatic polymer. The material for use at 193 nm has been found to be less sturdy than 248 nm photoresists when exposed to standard argon and C_4F_8 based discharges [2.10-2.11], as well as having an increased surface roughness [2.12]. The e-beam generated plasma was used to investigate the etching and surface roughening behavior of these 193 nm and 248 nm photoresist materials under identical environments for a variety of process conditions [2.13].

Initial studies of plasma-polymer interactions were performed on the effects of Ar and SF_6/Ar plasmas produced at very low plasma potential and high controllability (pulsed discharges, independent RF biasing). Our work focused on how the ion bombardment energy, neutral reactivity (fluorine), and a fluorocarbon (FC) overlayer affect plasma-photoresist interactions.

2.2. Experimental Set-up and Procedures:

2.2.1 Photoresists

The plasma-polymer interactions of two chemically different photoresists were compared in LAPPS. The two resists used were a 248 nm PR, which consists of an aromatic ring structure, and a 193 nm PR, which is a methacrylate main chain containing lactone and adamantane based functional groups (Fig. 2.1).

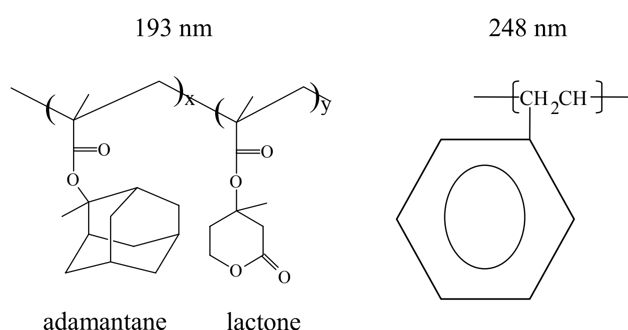

Figure 2.1 *Chemical Structures of 193 nm and 248 nm photoresist polymers.*

Both photoresist films were spin-coated to a thickness of about 410 nm on top of silicon substrates.

2.2.2 LAPPS

A schematic diagram of the LAPPS system is shown in Fig 2.2. The design and operation of LAPPS have been discussed previously both theoretically and experimentally [2.14-2.17]. Briefly, a linear hollow cathode (Fig. 2.2a) was used to generate a plane of high energy electrons which in turn generates a plasma layer described elsewhere [2.18]. The hollow cathode was driven by a 2 kV, 4 ms pulse operating at 20 ms period (typical). The generated e-beam passed through a slotted anode and terminated at a

grounded anode at the end of the chamber (Fig. 2.2b). A total gas flow rate of 50 sccm and a pressure operating range of 24 to 95 mTorr was used. A lower pressure was used in the pure Ar experiments to create the same ion current density at the substrate surface as measured for the SF_6/Ar experiments.

Additionally, a magnetic field 165 Gauss was applied by the Helmholtz coils to collimate the generated electrons and prevent spreading. A processing stage was located parallel along the beam axis of the plasma layer [2.19]. On the isolated electrode, a 5 cm diameter anodized aluminum plate (0.05" thick) was attached to the stage via screws. The photoresists were cut into 1 by 3 cm^2 samples and were adhered to the anodized sample holder via silver print epoxy. The stage face was located 2 cm from the center of the beam channel. The chamber had a base pressure below 8 x 10^{-7} Torr. A high vacuum turbomolecular pump was throttled with a manual valve to set the system's operating pressure.

The measurements of the RF voltage and currents to the stage were done in air at the electrical feed-through with a 10x oscilloscope probe and current transformer (Pearson Electronics Model 2877). Etching times corresponded to the pulse period (T_{on} + T_{off}) multiplied by the number of pulses. Pulse on times were held constant at 4 ms and the afterglow time (T_{off}) was varied from 16 to 300 ms. The stage temperature was kept at 22 ± 4 °C with a recirculating water bath during all experiments.

Standard conditions used during the processes were: T_{on} = 4 ms and T_{off} = 16 ms with a total run time of 12.5 minutes, and a gas flow rate of 50 sccm. Additionally, the hollow cathode was pulsed at 2 kV, and an RF bias of 50 V (dc selfbias voltage) was applied to the stage. Typical operating pressure for the Ar experiments was about 25

mTorr, and for SF_6/Ar experiments was fixed at 95 mTorr. We chose to keep the ion current densities the same, rather than the pressure, for different experiments.

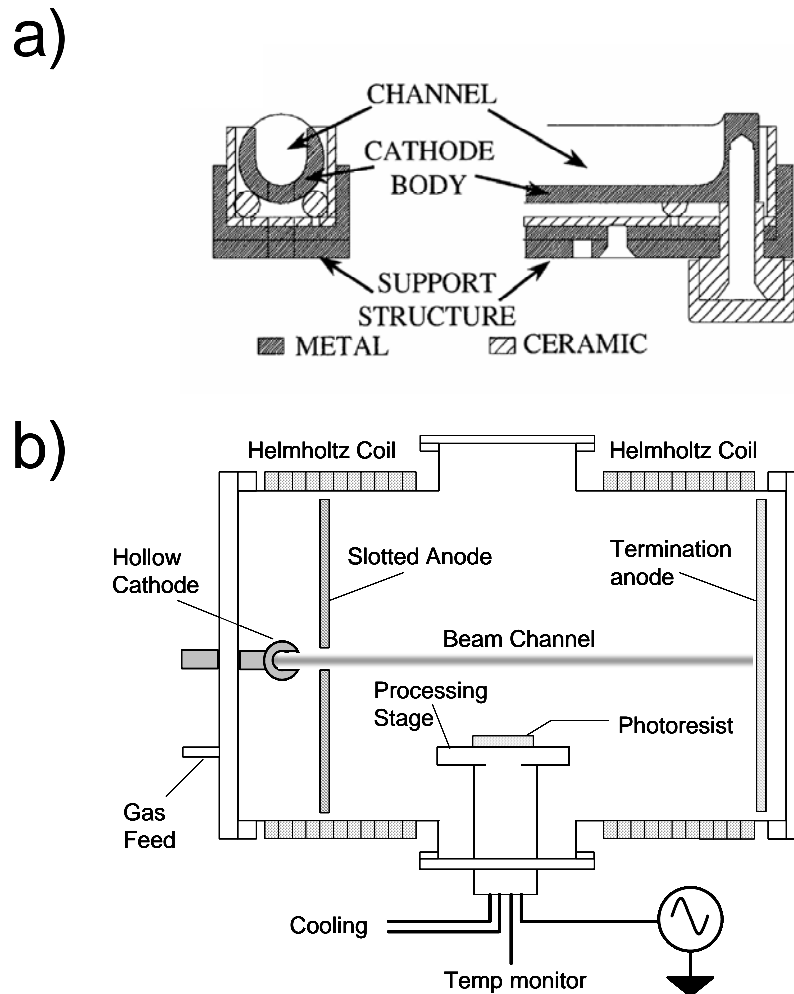

Figure 2.2 *Schematic diagram of LAPPS. a) Cross sectional detail of linear hollow cathode construction b) schematic of etching chamber.*

2.2.3 Ex Situ Analysis

Film thicknesses were determined using an automatic ellipsometer with a 632.8 nm He–Ne laser [2.20, 2.21]. The change in film thickness was used to determine etch depth (ED), thin film etching rates, and the introduction of surface modifications. The ED was

then divided by the total run time and used to calculate the etch rate ((ER) = ED/run time). Surface roughness was studied using a Digital Instruments BioScope AFM, *ex situ*. All of the AFM scans on the samples were done over an area of 1 μm^2, at a scan rate of 1 Hz.

2.2.4 Thin FC layer

The thin FC layer was added to the samples using a capacitively coupled plasma system described elsewhere [2.22]. Briefly, the deposition used remote C_4F_8 or C_4F_8/90%Ar plasmas with a roof structure over the samples [2.13,2.23-2.24] and the deposition times were 1, 2, 5 and 10 minutes. The depositions were run at 30 mTorr with a 40 sccm total gas flow rate, and the stage was unbiased. The samples were analyzed using ellipsometry and AFM. FC films deposited in this way were typically 0.5 nm to 4 nm in thickness as measured by ellipsometry, and surface roughness values will be reported below.

2.3. Results

A purely physical etching mechanism (Ar only) and one with a chemical etching component (5%SF_6/Ar) were studied to delineate the differences in impact on etching behavior and surface evolution of the two PRs. The surface roughness characteristics and etch rates of the two PRs as a function of RF bias voltage are shown in Fig. 2.3. These experiments were performed at standard conditions but the bias voltage was changed (grounded to 10 V to 50V). The pressure for the Ar plasma was adjusted slightly for the different RF bias conditions (~24 to 25 to 27.5 mTorr) and the 5%SF_6 was held constant at 95 mTorr, which yielded the same ion currents to the stage. Figure 2.3 shows that the photoresist etch rates monotonically increased with the RF bias voltage, whereas the

surface roughness seemed to saturate for the pure Ar experiments. When SF_6 was added to the Ar plasma (solid symbols), the measured surface roughness was greater than for a pure Ar plasma (open symbols), and a noticeable effect of the RF bias on surface roughness. Although the two photoresists showed qualitatively the same trends when exposed to different plasmas, Fig. 2.3 shows that the 193 nm PR has a greater RMS roughness than the 248nm material, and a greater etch depth.

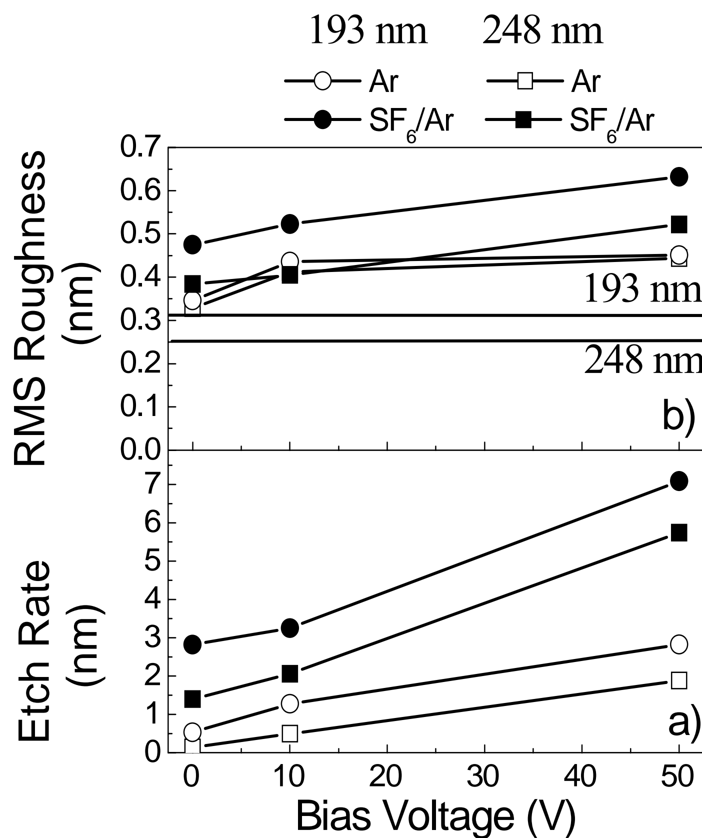

Figure 2.3 *a) Etch rate as a function of RF bias in pure Ar and 5% SF_6/Ar electron-beam generated plasmas. b) RMS roughness at varying bias voltages for Ar and 5%SF_6/Ar plasmas. Virgin photoresist RMS roughness are shown for the 193 and 248 nm PR. The pressure was 95 mTorr for all SF_6 experiments and the pressure for Ar changes from 24 to 25 to 27.5 mTorr with increasing bias voltage which gave the same ion currents at the wafer stage. All other experimental parameters were at standard conditions.*

2.3.1 Effect of Fluorine addition

A set of experiments were conducted to examine the overall effect of fluorine addition on the surface modifications in comparison to purely physical etching (Ar). These experiments were conducted with an RF bias of 10V. Figure 2.4 shows that as the percentage of SF_6 increased in the Ar/SF_6 gas mixture, the etch rate also increased. Figure 2.4 also shows that the surface roughness increased slightly with increasing fluorine content. As noted above the 193 nm PR has a greater etch rate and RMS roughness compared to the 248 nm PR.

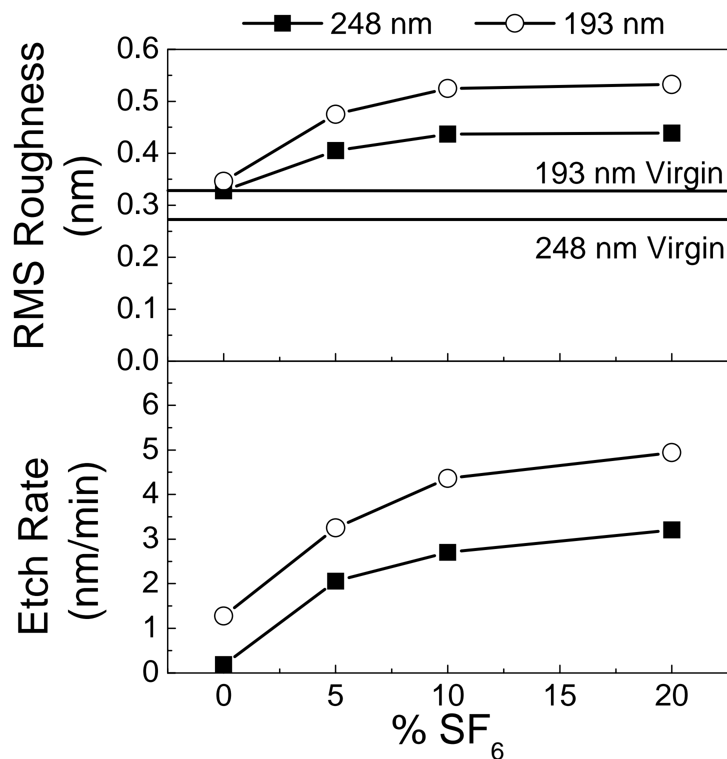

Figure 2.4 *a) The 193 nm and 248 nm photoresist etch rates at varying percentage of SF_6 in Ar plasma. b) The RMS roughness at varying percentage SF_6. The samples were run at equivalent ion currents and a 10V applied bias.*

In general we found in this work that the RMS roughness increased with the etching depth. This was further investigated by studying the RMS roughness introduced per nm of PR etched for different process conditions (Fig 2.5). The amount of RMS roughness introduced per nm of photoresist etched with an SF_6/Ar plasma is greatly reduced over physical sputtering (pure Ar) for the same RF bias voltage. However the difference between the different gas chemistries is reduced for increasing RF bias voltages. Additionally, the amount of RMS roughness introduced per nm of photoresist etched is reduced for 193 nm PR relative to 248 nm PR material, even though the overall surface roughness is greater for the 193 nm PR. This was due to the greater etching depth of the 193 nm material relative to the 248 nm material.

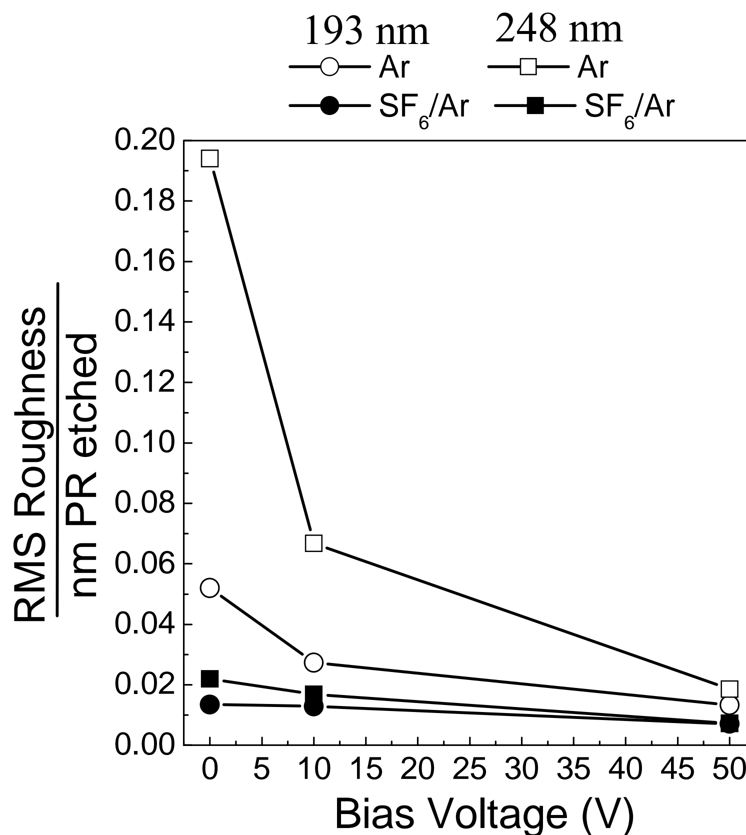

Figure 2.5 *The RMS roughness per nm PR etched versus RF bias voltage. The samples were run at standard conditions expect for the applied bias. The operating pressure for the pure Ar plasmas were 24 to 25 to 27.5 mTorr with increasing bias voltage, and the 5%SF6/Ar plasmas were run at 95 mTorr to keep the ion currents the same for different experiments.*

Since LAPPS is a pulsed discharge the effect of changing the pulsing conditions on the PR's surface evolution was studied. This was accomplished by varying T_{off} for fixed T_{on} (4 ms) at 10 V bias voltage using 5%SF_6/Ar plasma (Fig. 2.6). The etch depth per pulse and the surface roughness changed as a function of T_{off}. Especially for the 193 nm photoresist material there is a continued etching and an increase of the surface roughness for greater afterglow period (Fig 2.6). For the 248 nm material there appears to be a saturation of the etching depth per pulse and the RMS roughness at T_{off} of about 100 ms, and may be indicative of a chemically less reactive polymer structure.

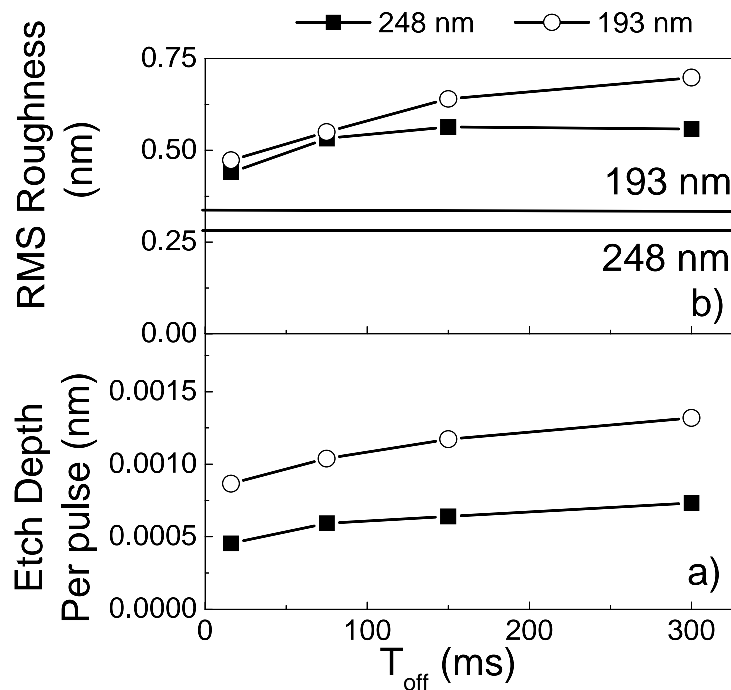

Figure 2.6 *a)5% SF6/Ar plasmas showing the effect on etch depth per pulse and b) RMS roughness of varying pulse afterglow times for T_{on} = 4 ms. Experiments were performed at otherwise standard conditions with a 10 V applied bias.*

2.3.2 Thin FC layer

It is well known that selective SiO_2 etching is possible through FC polymer deposition and is strongly dependent on the ratio of fluorocarbon radicals to atomic

fluorine [2.25 - 2.29]. Experiments were conducted to study the effect of a preexisting thin FC layer on PR surface evolution and to investigate differences from pure Ar and SF_6/Ar discharges. AFM images obtained with a 193 nm PR with either a thin or thick FC layer, deposited using either C_4F_8/90%Ar or C_4F_8, before and after LAPPS exposure to pure Ar discharges, respectively, are shown in Fig. 2.7. Properties of deposited FC films have been described by Zheng, and also by Ling [2.13, 2.24, 2.30]. For the samples shown in Fig. 2.7, the FC layers were deposited for 5 minutes, and then etched at 50 V bias in pure Ar. After etching of both the FC layer and the PR underlayer, the resulting PR surface roughness appeared to be reduced relative to the initial FC layer roughness, but the overall roughness values were larger than seen for PR without an FC layer.

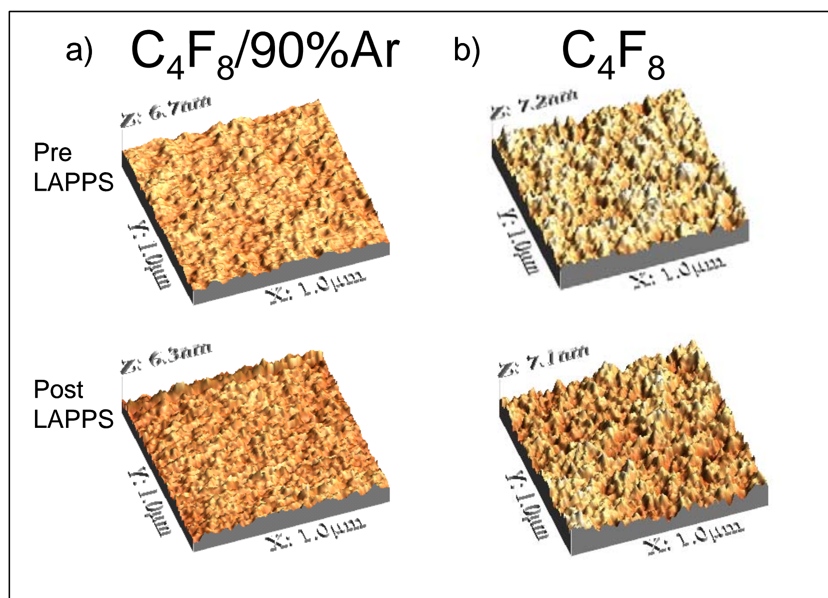

Figure 2.7 *AFM images of blanket FC films deposited on 193 nm photoresist before and after Ar etching. (a) C_4F_8/90%Ar FC deposiion (b) C_4F_8 FC deposition. Pre and post Ar plasma LAPPS exposures at 50 V RF bias are shown for both situations.*

Figure 2.8 shows the effect on the PR etch depth and RMS roughness post LAPPS exposure (50 V bias in a pure Ar plasma) at various FC layer thicknesses (pure C_4F_8). Data obtained without FC layer are also shown. The PR etch depth is the net etching

depth of the PR film, without considering the removal of the FC film. For both PRs the etch depth was dependent on the deposition time (film thickness, Fig. 2.8). There was also an increase in the surface roughness at longer FC deposition times, but for very large initial FC film thicknesses ~4 nm, and RMS roughness, the roughness of the etched PR underlayer is reduced relative to the initial FC layer roughness.

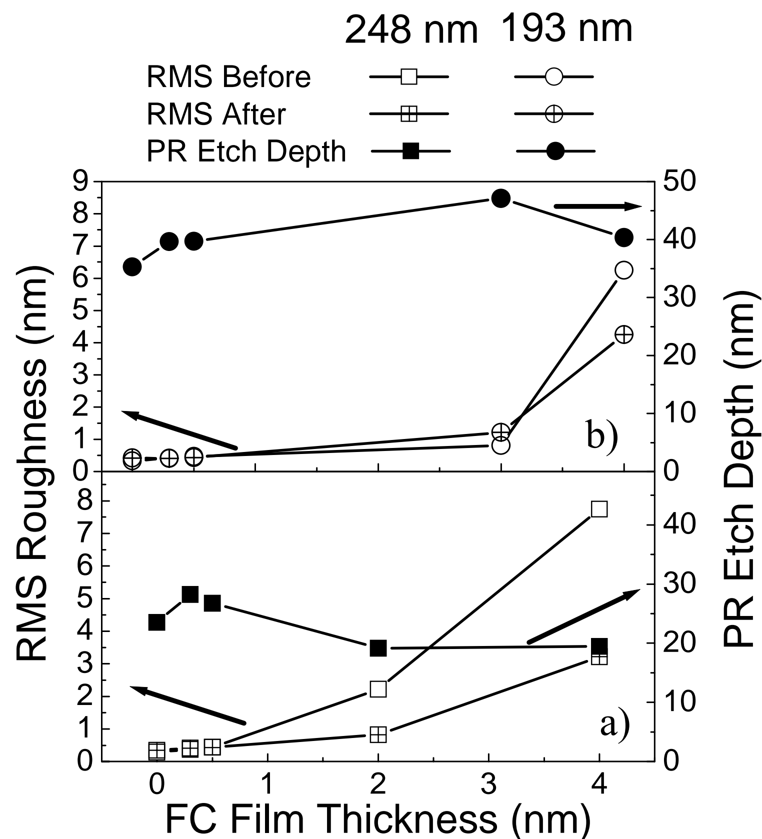

Figure 2.8 *a) RMS and PR etch rate of C_4F_8 deposited FC layer/PR in an Ar plasma as a function of FC film thickness for 248 nm PR's b) Same for C_4F_8 deposited FC layer/193 nm PR stacks. The experiments were run at standard conditions using pure Ar.*

The effect of thinner FC layers produced using C_4F_8/90%Ar deposition gas chemistry was also studied. Figure 2.9 shows how the PR etch depth and RMS roughness changes as a function of film thickness in a pure Ar plasma at 50 V bias. Results for PR samples without a FC layer are also shown. An increase in the surface roughness at

longer FC deposition times is seen in Figure 2.9, and little change before and after LAPPS exposure for the RMS roughness. Again, a smoothing effect for both PR materials was seen for the thickest FC layer employed. However, the amount of etching of the PR seems to follow the RMS Roughness of the FC layer.

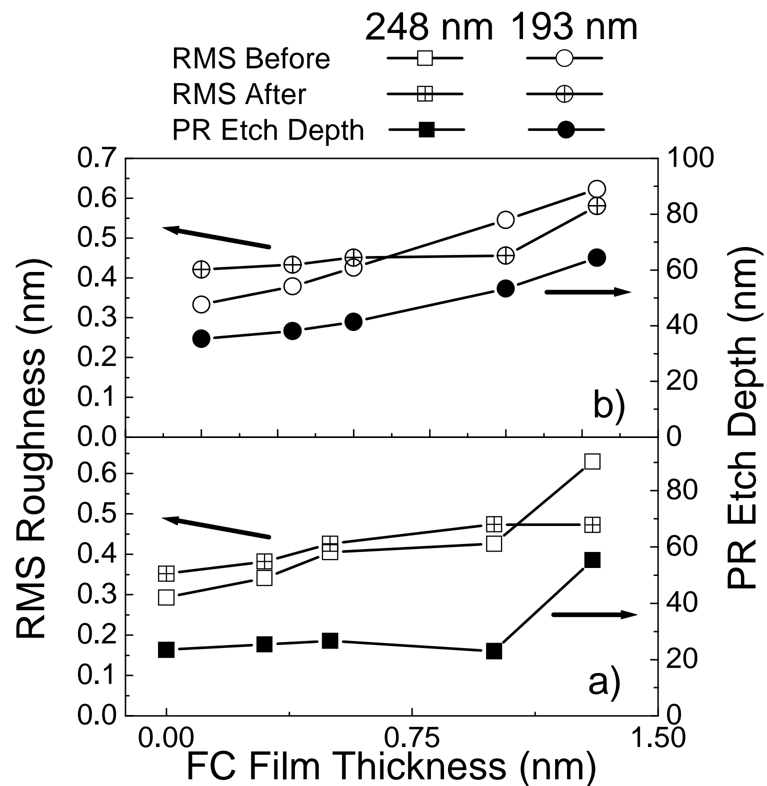

Figure 2.9 *a) RMS and PR etching depth of a C_4F_8/90%Ar FC layer/248 nm PR stack in an Ar LAPPS plasma as a function FC thickness. b) Same for C_4F_8/90%Ar deposited FC layer/193 nm PR stacks. The experiments were run at standard conditions using pure Ar.*

2.4. Discussion:

The reduced plasma potential of LAPPS enabled us to study PR etching and surface roughness evolution at very low ion energies. Our results indicate that there was finite photoresist etching in pure Ar without RF bias and low plasma potential (less then

5 eV in the pure Ar system), and that the etching rate of 193 nm PR was higher than that of 248 nm PR. Without RF bias, this enhanced etching should be dominated by deposition of the energy corresponding to the ionization potential of Ar^+, and possible deexcitation of metastables.

The addition of fluorine to the discharge gas was also explored at low plasma potentials. At a fixed bias of 10 V, the etch rate increased with the percentage of SF_6, and showed that a greater amount of fluorine was able to interact with the surface and aid the etching (Fig 2.4). Again, this chemically enhanced etching took place at a higher rate for the 193 nm PR material than for the 248 nm PR.

Surprisingly, the RMS roughness per nm etch depth introduced is slightly greater for the 248 nm PR than the 193 nm PR (Fig 2.5). The roughness per nm etch depth is also greater for a pure Ar plasma than for an SF_6/Ar discharge (Fig 2.5). This seems to indicate that the fluorine-related attack contributes more to the etching, than to enhancing the roughness of the PR surface. The pulsed nature of LAPPS was useful to examine this aspect of the etching characteristics. By changing the afterglow (T_{off}) in 5%SF_6/Ar discharges, we find that the RMS roughness continues to increase for the 193 nm PR, while the 248 nm PR saturates (Fig. 2.6). This is consistent with the notion that the 193 nm is both more reactive than the 248 nm PR, and that some surface roughness is associated with PR etching, even for the afterglow, which should be dominated by the attack of long-lived neutral species. Thin FC films increased the etch rate of the PRs, however no significant change in the RMS roughness was introduced between a PR with a small (< 1 nm) FC layer and one without. Very large FC depositions (4 nm) resulted in large RMS roughness values, however, during subsequent LAPPS exposure there was a

smoothing of that film's roughness. Therefore, although FC film related surface roughness can be reproduced in photoresist underlayers, and we observed that as the FC thickness increased there was an increase in RMS roughness values (Fig 2.8 and 2.9), there is not a 1-to-1 correspondence of FC film roughness and resulting PR roughness for FC film thicknesses varied over a significant range.

2.5. Conclusions:

In these experiments we have examined the effects of ion bombardment energy for pure Ar discharges, the effect of chemical reactants (fluorine addition to Ar plasma) and the presence of a thin FC layer on blanket etching rates and surface roughness of 193 nm and 248 nm photoresist materials. Low energy ion bombardment caused an appreciable and reproducible increase in the roughness of the photoresist surfaces. When small amounts of fluorine were added using SF_6/Ar gas mixtures, we observed an increase of the etch rate and the surface roughness. However, the amount of surface roughness per nm of PR etch depth in a fluorinated plasma was decreased over that of a pure Ar plasma. Further it was shown that the roughness of a deposited FC layer in the nanometer thickness range can impact the surface roughness of the etched PR underlayers, but that this effect is dependent upon the initial FC layer thickness and roughness.

Acknowledgements

This work was supported by the Office of Naval Research. G. S. Oehrlein's contribution to the work was supported in part by the National Science Foundation under Grant No. 0406120.

Chapter 3: Temporal behavior and Fluence changes in LAPPS during photoresist etching

3.1 Introduction

As previously noted, LAPPS is a pulsed system, which allows additional capabilities that may be used to further enhance process control and quality. The "steady state" in modulated plasmas, if achieved at all, represents only a fraction of the processing time. Over the course of one period, the plasma undergoes distinct phases that lead to unique and potentially useful changes in the flux of species at processing surfaces. Given these changes, it is useful to characterize the effect of varying the pulse period, T_{on} and T_{off}, in order to better control the surface morphology, and have an additional quality control parameter. This chapter discusses experiments using electron beam-generated plasmas produced in argon with the goal of developing an understanding of the temporal behavior of the system.

3.2 Experimental Setup

The experiments conducted to elucidate the temporal behavior of LAPPS closely follows the set up described in chapter two. The biasing technique, analysis, and data gathering techniques were the same, however additional experiments were conducted in a different chamber which is described below. The two well characterized photoresists (193 nm and 248 nm) were used for exploring the importance of the temporal behavior and fluence differences in LAPPS.

3.2.1 Photoresists

The plasma-polymer interactions of two chemically different photoresists (PR) were compared in LAPPS. The two resists used were a 248 nm PR, which consists of an aromatic ring structure, and a 193 nm PR which is a methacrylate main chain containing lactone and adamantane based functional groups (Fig. 3.1).

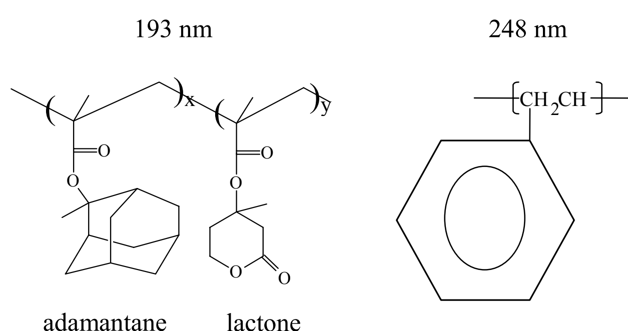

Figure 3.1 *Chemical Structures of 193 and 248 nm photoresist materials*

Samples were received with a spin on coating process and hard bake. Both PR samples were ~ 410 nm in thickness on top of a silicon substrate.

3.2.2 Argon Experiments (SS chamber)

Initial experiments were conducted using an Ar plasma in a stainless steel (SS) chamber (Fig. 3.2) and involved changing the bias, the pulse durations (T_{on} 1 – 7 ms), and the afterglow (T_{off} 16 – 300 ms) of the system. A processing pressure of 95 mTorr was used with a flow of 50 sccm of Ar (99.999% purity), while all other processing conditions were the same as described in Chapter 2 (Section 2.2.2). The SS chamber contained a vertically oriented e-beam, and used a diffusion pump backed by a rough pump with a base pressure of 7 x 10^{-7} Torr.

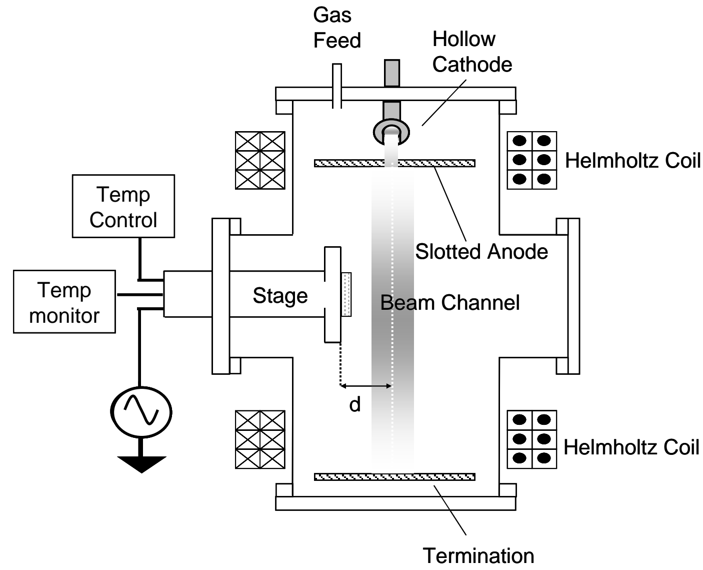

Figure 3.2 *Schematic diagram of LAPPS set up used for the temporal experiments (Stainless Steel chamber).*

3.3 Results

Figure 3.3 shows an example of the timing sequence and subsequent etch rates for the pulsed LAPPS. The cathode voltage (e-beam duration) was applied during the T_{on} time. During the T_{on} time the PR etch rate was maximized. During the afterglow (T_{off}), etching continued, albeit at a slower rate.

.

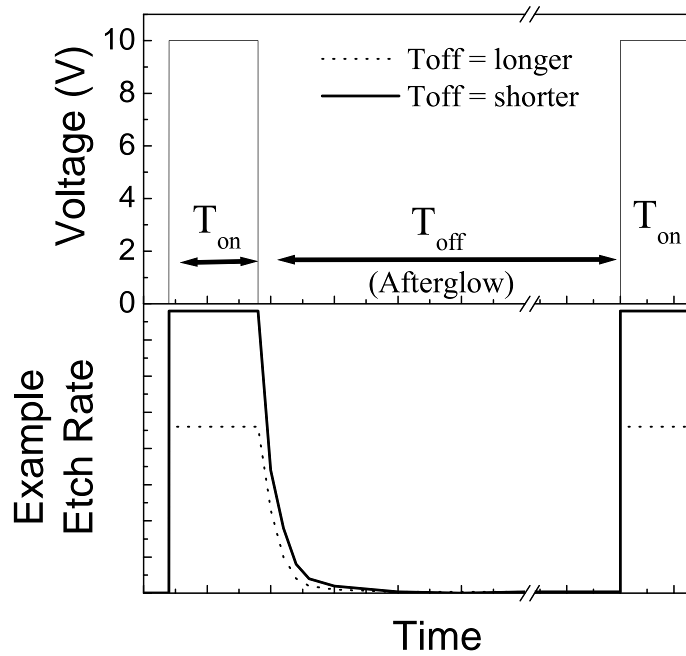

Figure 3.3 *Schematic of LAPPS operation showing the voltage and etch rate vs time.*

The analysis used to characterize the etch rates for T_{on} and T_{off} is shown in Fig 3.4. The etch depth for a continuous plasma was found by extrapolating T_{off} to zero on the etch depth (ED) vs T_{off} plot. This etch depth during the pulse (T_{on}) is shown as ED_{on}. The ED_{off} contribution was calculated by ED_{total} - ED_{on} (Fig 3.4). Etch rates were then calculated by dividing the etch depths (ED_{on} and ED_{off}) by the time ("pulse" T_{on} and "afterglow" T_{off}) i.e. $ER_{on} = ED_{on} / T_{on}$ (nm/min) and $ER_{off} = ED_{off} / T_{off}$ (nm/min).

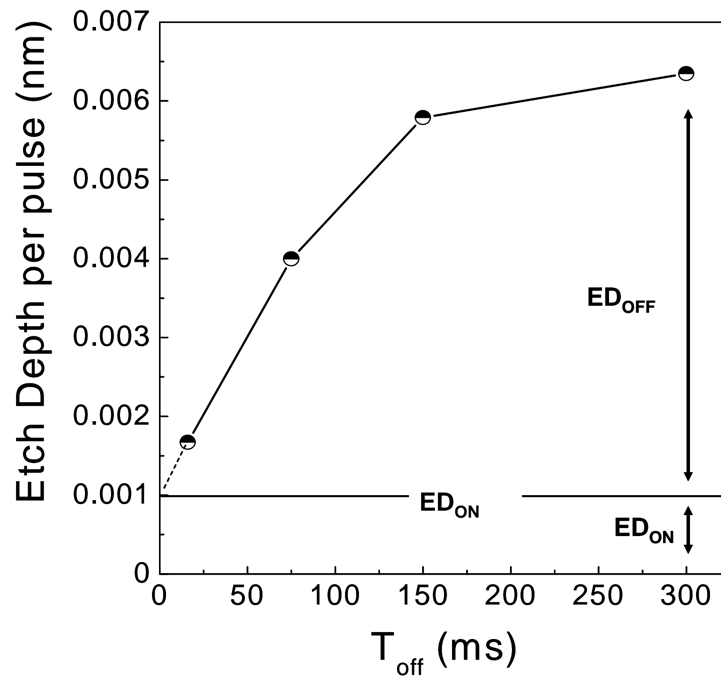

Figure 3.4 *Standard analysis of photoresist etching: temporal dependencies.*

The dependence of the 193 nm etch depth per pulse as a function of T_{on} and T_{off} is shown in Fig. 3.5. A bias of 10 V was used for etching in the SS chamber during these experiments. The 248 nm PR showed a similar trend in etch depth per pulse as a function of T_{on} and T_{off} (data not shown). The etch depth increased with both the pulse (T_{on}) and afterglow (T_{off}) times. The etch depth per pulse seemed to reach a limit as T_{off} increased. The largest increase to the etch depth per pulse occurred at a pulse of 7 ms.

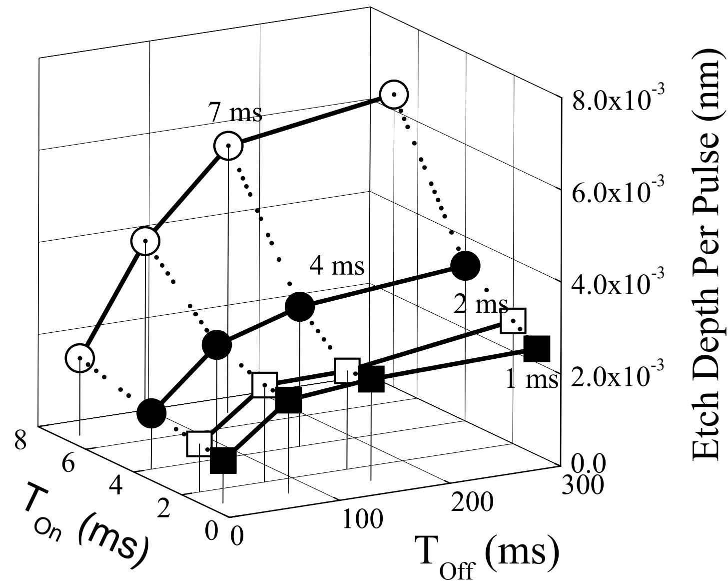

Figure 3.5 *193 nm PR plots of etch depth per pulse as a function of T_{on} and T_{off}. Processing was done in the SS chamber with a 10 V bias and a pure Ar discharge.*

The RMS roughness per pulse for the 193 nm PR is shown in Fig 3.6. The 248 nm surface roughness showed similar trends in surface roughness to the 193 nm PR; however the overall RMS roughnesses were greater than the 193 nm PR (data not shown). RMS roughness increased with the pulse length and afterglow. There appeared to be a limit for the roughness at T_{off} = 100 -150 ms regardless of the T_{on} period.

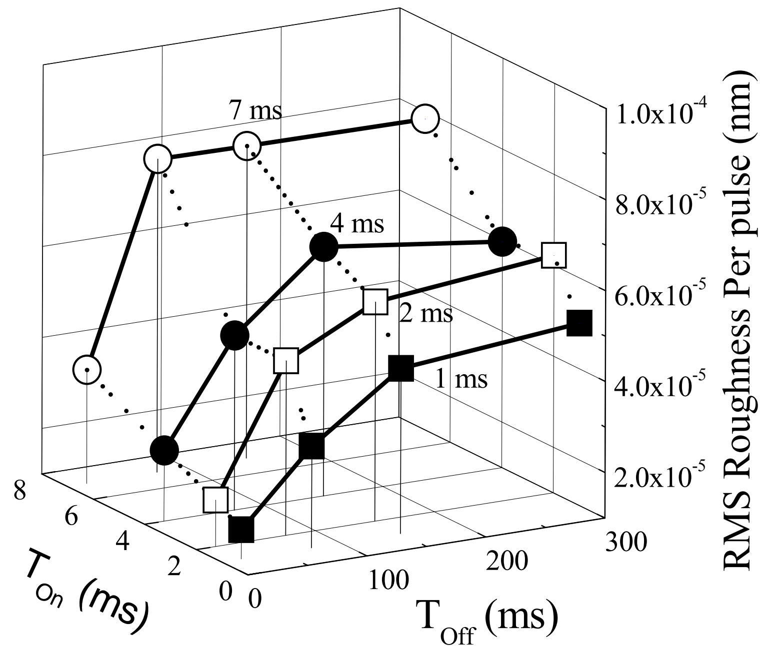

Figure 3.6 *193 nm PR plots of RMS roughness per pulse as a function of T_{on} and T_{off}. Processing was done in the SS chamber with a 10 V applied bias and a pure Ar discharge.*

The etch rates of the 193 nm PR as a function of T_{on} (at a constant T_{off} of 300 ms) are shown in Fig. 3.7 for the same process conditions (SS chamber, 10 V bias). Since the etch rate from the afterglow was significantly lower, Fig. 3.7 was plotted on a semi-logarithmic scale. The T_{on} etch rate decreased as a function of the pulse width.

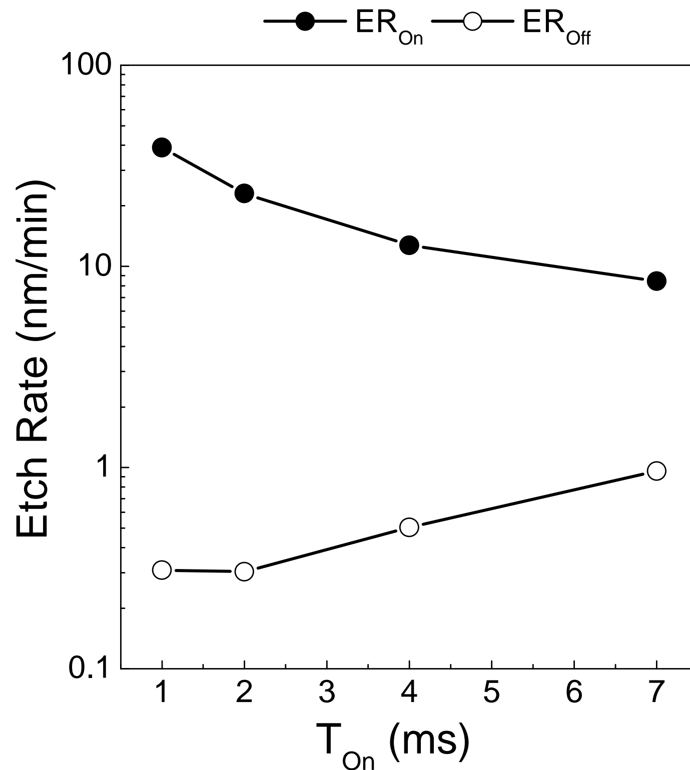

Figure 3.7 *193 nm PR etch rate as a function of T_{on}. Processing done in the SS chamber with a 10V applied bias, T_{off} of 300 ms, and in a pure Ar discharge.*

The RMS roughness and etch rate as a function of bias voltage in the SS chamber and T_{on} = 4 ms and T_{off} = 16 ms is diagramed in Fig 3.8. The etching was done at bias voltages of 0, 10, and 50 V with a total run time of 25 minutes. A greater bias voltage lead to an increased etch depth and etch rate. Figure 3.8 also shows that the RMS roughness saturated immediately at ~1 nm value.

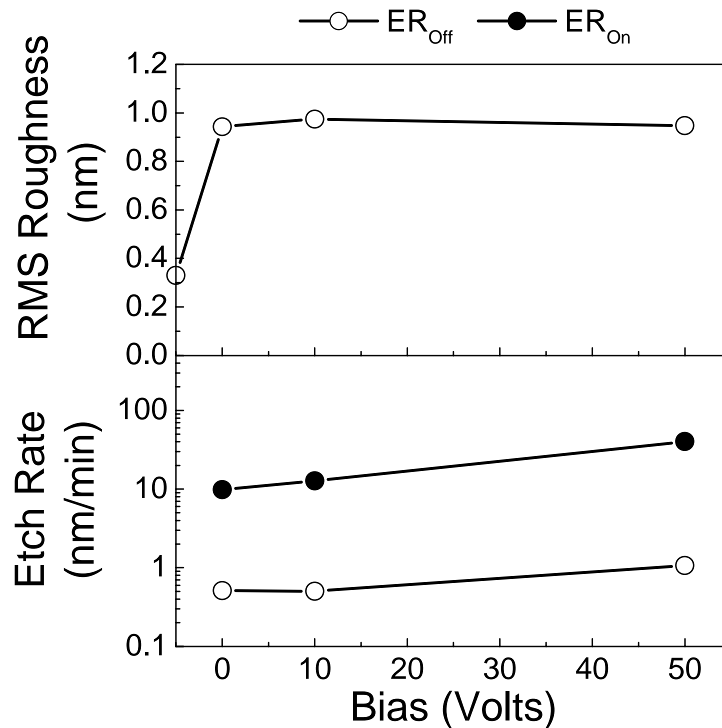

Figure 3.8 *193 nm PR plots of RMS roughness and etch rate as a function of bias. Processing done in the SS chamber with a total run time of 25 min and in a pure Ar discharge. The RMS roughness corresponding to ~0.33 is the unexposed PR roughness.*

3.4 Discussion

LAPPS was used to study the effects of the plasma-polymer interactions in pure Ar. An effect on the pulse width and afterglow was seen. A greater amount of etching per pulse occurred for both 193 nm and 248 nm PRs at longer T_{on} times. A similar trend occurred for longer afterglows (T_{off}). The same trend also occurred for the surface roughness, however, for $T_{off} \geq 150$ ms the surface roughness reached a limit. Ion bombardment lead to a roughening of the surface and was energy (bias voltage) dependent. The etching and surface roughness was increased by a chemical etch component on the PR.

3.4.1 Effect of pulsed LAPPS

There was a temporal dependence of the surface roughness, etch depth, and etch rate on T_{on} and T_{off} for both photoresists. The mechanistic origin of the differences in response behavior of the PRs was investigated by exploring the changes with Ar plasma at very low plasma potential and high controllability. The primary etching during the pulse (T_{on}) can be attributed to the ion bombardment. However, the additional etching, with respect to T_{off} may be the result of the creation of radicals at the surface by the impact of plasma generated ions, or long lived oxygen radicals present in the chamber. There is a finite lifetime of these generated radicals from the surface, such that at long T_{off} times (300 ms) the radicals are no longer present and the additional etching is reduced. The plasma gas chemistry also affects the lifetimes of the specific ions generated. For Ar based plasma chemistries the ion lifetimes have been reported to be long (~145 ms) [3.1] in comparison to SF_6 based plasmas, where the ion lifetimes are reported to be a maximum of 10 ms [3.2]. This difference in ion lifetimes did not show a significant effect on the overall etching during the afterglow. However, etching during the afterglow may be caused by the gas constituents in the chamber because of their long residence times (~ 20 sec). Because of the long residence times of radicals, including metastables and fast neutrals, they may contribute to the etching during the afterglow. The effect of T_{on} on the etch depth per pulse follows a linear trend, i.e. greater T_{on} times result in greater etch depth implying a purely ion driven process.

The surface roughness initially increased as the afterglow time increased (Fig 3.6). However, a limit was reached as the afterglow was lengthened. One observation is that the surface evolved during the plasma off time in the Ar plasma. By using the two

different polymers, the evolution of the reactivity of the two PR materials can be studied. A novel observation made during the experiments was that the surface roughness of the 248 nm PR was greater compared to the 193 nm PR in the SS chamber, although the 248 nm PR etch rate was still lower than the 193 nm PR etch rate as seen previously [3.3, 3.4]. In addition, at long T_{off} times (300 ms) the roughness decreased, implying an annealing of the damage during the afterglow. Since the plasma potential (V_{pl}) is significantly higher in conventional plasmas than in LAPPS, the incident ion energy is greater ($E_{ion} = e(V_{bias} + V_{pl})$) and thus the roughness was observed to increase [3.3]. Because lower bias voltages were applied during the experiments using LAPPS, the amount of roughness could be reduced over traditional plasma systems.

We suggest that the annealing of damage during the afterglow is responsible for the observed limit in the surface roughness. During the plasma off time, the bonds in the photoresist are able to rearrange and form new bonds, and in essence anneal itself before the next etching cycle began. However, the 248 nm material appeared unable to "cure" itself, probably due to the rigid aromatic ring structure of the 248 nm PR, which can prohibit the movement or rotation of the bonds and potentially prevent the curing of the damaged surface.

By increasing the T_{on} time, more material was 'physically' removed and subsequently damaged by ion bombardment, thus increasing the surface roughness. The overall trend of the surface roughness showed a dependence on both T_{on} and T_{off}. The amount of etching contributed by the T_{on} decreased with the pulse width, implying an possible ignition phenomena, while the etching corresponding to T_{off} increased. In addition, the effect of the afterglow etching (ER_{off}) was much greater at longer T_{on} pulses

(Fig 3.7). However, the total amount of etching contributed over the total time period decreased due to the fact that during the pulse period (ER_{on}) the ER decreased. Thus the behavior is more closely coupled to the effect of T_{off} than T_{on}. Our results are similar to those results of Law et al. [3.5] who reported that the increase of pulse width resulted in a lower etch rate.

The greater bias voltages lead to an increased etch rate while the roughness immediately saturated (Fig. 3.8) for the pure argon system. Similar to the low bias voltage case (Fig. 3.5), we suggest that the annealing of damage during the afterglow is responsible for the observed limit. A comparison of experiments of ion driven mechanisms to that of chemical etching (fluorine) mechanisms may aid in understanding the initial mechanisms on the etch rate and roughness of the two PRs. For direct comparisons, experiments at equivalent ion currents are necessary in order to analyze the two constituents (ion bombardment and chemical). These results were discussed in section 2.4.4

3.4.2 Ar^+ Ion Bombardment

Very little surface roughening was observed with LAPPS. This may be explained by the low ion fluence and low ion energies achieved with LAPPS. The amount of etching observed appears to scale with the energy of the incident ions striking the surface. The etching increased by 50 % from no bias to 10 V, and increased by a factor of three when the bias is raised to 50 V (Fig 3.8). Since 248 nm PR is more stable and can absorb stronger impacts without undergoing bond cleavage (C=C bond energy ~6.4 eV vs 3.6 eV for a C-C bond, Figure 3.1), we would expect the 248 nm PR etching to be less compared to the 193 nm PR. Since the V_{pl} and V_{bias} are known, the amount of energy applied to the

surface can be delineated with a better degree of control. The plasma potential of LAPPS was very low ~ 5 T_e or 6 V. It is important to note that for Ar plasmas $T_e \approx 1$ to 1.5 eV, $V_{pl} \approx 5$ to 7 V and $E_{ion} \approx 5$ to 7 eV, however, when a molecular gas is added T_e is reduced to ≈ 0.5 eV, $V_{pl} \approx 2$ V and $E_{ion} \approx 2$ eV [3.6-3.9].

Another explanation for the increased etching during the afterglow may be the possible role of long lived oxygen radicals in the system. It is known that even small amounts of oxygen greatly enhance the etching rate of the photoresists, and that this can be one of many mechanisms of etching during the afterglow.

3.4.3 Fluence

The etching yields for the two PRs are displayed in Table 3.1. The amount of RMS roughness was increased based upon the material etching characteristics and the fluence to the substrate surface. The observed differences in the etch yields between the two chambers (Al and SS) may be caused by the varying fluences of reactive species at the surfaces. The surface evolution in the Al chamber is considered in a non-steady-state regime because of the presence of water vapor (more specifically the oxygen) that was deposited on the samples and resulted in faster etching. The resulting etching yield is increased over that which occurs in the SS chamber, due to a lower fluence, and a much lower amount of etching taking place.

Conditions	RMS Roughness (nm/10^{16} ions/cm^2) 193 nm	RMS Roughness (nm/10^{16} ions/cm^2) 248 nm	Etch Yield (amu/ion) 193 nm	Etch Yield (amu/ion) 248 nm
SS chamber Ar Grounded	7.09E-03	1.14E-02	0.637	0.545
SS chamber Ar 10V bias	7.33E-03	1.34E-02	0.853	0.644
SS chamber Ar 50V bias	7.12E-03	1.51E-02	2.194	1.582
Al chamber Ar Grounded	1.02E-01	9.68E-02	4.72	1.201
Al chamber Ar 10V bias	1.29E-01	1.22E-01	11.314	4.385
Al chamber Ar 50V bias	1.33E-01	1.31E-01	25.09	16.694
Al chamber 5%SF6/Ar Grounded	1.40E-01	1.13E-01	24.92	12.394
Al chamber 5%SF6/Ar 10V bias	1.54E-01	1.20E-01	28.89	18.762
Al chamber 5%SF6/Ar 50V bias	1.86E-01	1.80E-01	62.97	51.521

Table 3.1 *Calculated etch yield and RMS roughness as a function of fluence for various conditions.*

In the SS chamber, the operating pressure was 95 mTorr and resulted in etch yields that are closer to steady state conditions, which was due to the lower base pressure of the chamber and, therefore, reduced presence of water vapor. Hence, the fluence between the two operating chambers was different. The etch yield of 1.582 amu/ion in the SS chamber is similar to what Doemling reported in an ICP: an etch yield of 0.5 amu/ion at 50 V [3.10]. In order to maintain a constant ion current between the various gas chemistries, an overall lower fluence was used in the Al chamber (Chapter 2). It is this change in the fluence that is responsible for the changed etch yield between the two chambers. The etch yield in the fluorine-chemistry based Al chamber was substantially higher (~17 amu/ion) than steady state etch yields reported in traditional plasma systems [3.10]. This implies that there may have been non-steady-state conditions in the Al chamber. There are other factors that can also influence the etch yield in all plasma

systems. For instance, fast neutrals have been reported to enhance etch yield [3.11-3.12]. For all plasma systems, including LAPPS, this can not be avoided [3.13]. There is also the effect of water vapor that is initially deposited on the PR film when the PR is exposed to air. This adsorbed water vapor (increase in oxygen) initially increases the etch yield at the surface before saturating and reaching a steady state. The impact of different fluences to the surface affects the amount of total etching involved and shows that the etch yield is greatly increased in the Al chamber over the SS chamber, and that the RMS roughness per 10^{16} ions/cm^2 is increased (Table 3.1).

3.5 Conclusions

Low energy ion bombardment resulted in an increase in the surface roughness with longer pulse on time (7 ms) and afterglow periods (150 to 300 ms). The fact that the PR surface roughness evolved during the afterglow of an Ar plasma was an unexpected result. The surface evolution continued during the afterglow period but decreased for long afterglow times (300 ms) for the 193 nm PR. This might be explained by the ability of the material to cure itself before the next etching cycle.

Even low energy ion bombardment (below the plasma potential of many systems) caused an appreciable increase in the surface roughness. Our experiments indicate that there was a large dependence of the ion energy on the surface morphology. There also appeared to be a difference in the response of the PR with regard to the fluence. A large fluence allowed the surface to reach steady state etching quicker. However, at lower fluences there was a large increase in the etch yield (an order of magnitude), but the RMS roughness was greatly reduced.

Chapter 4: Conclusions

An electron beam generated plasma processing system (LAPPS) was used to study plasma-polymer interactions between PR that differed significantly in polymer structure. The effects of Ar^+ ion bombardment energy, chemically-assisted etching using fluorine, and the presence of a thin FC layer were examined through the surface roughness evolution and etching rates of blanket 193 nm and 248 nm photoresists. LAPPS provided a good test system to de-convolute plasma-polymer interactions. The surface evolution was dependent on the plasma modulation as well. An increase in T_{on} or T_{off} raised the amount of etching and surface roughness. A novel observation made during the course of the experiments was that the surface evolution continued into the afterglow period. At long T_{off} times for 193 nm materials there was a slight decrease in the surface roughness. This may be explained by the ability of the material to cure itself before the next etching cycle. With these experiments we were able to explore some interesting concepts into etching behavior that were previously unattainable. Even low energy ion bombardment (below the plasma potential of many systems) caused an appreciable increase in the surface roughness. In addition, by adding relatively small amounts of fluorine, we were able to establish that there was an increase in the surface roughness as well as the etch rate over pure ion bombardment. There was a reduction in RMS roughness introduced per nm of photoresist etched as a function of fluorine addition. However, this difference decreased with increasing ion energy. This chemical etching effect was also observed when a small FC layer was deposited on top of the samples and etched in a pure Ar plasma. We further observed that the roughness of the FC layer does impact the PR underlayers and is dependent upon the conditions of the FC deposition. For repetitive

etch/deposition processes that rely on FC layers to protect sidewalls, these limitations are important for the ultimate final critical dimensions. Increased control of the molecular-level plasma-photoresist interactions and the ability to understand how the surface roughness and etching of photoresists occurs will lead to a more precise control of the critical dimensions of future applications. Finally, the ability to link these aspects with a pulsed plasma also provides increased control over the variable characteristics that will be needed in the future.

References:

Chapter 1:

1.1 B. Singh, J.H. Tomas III, and V Patel, Applied Physics Letters 60, (1992) p 2335
1.2 J.C. Forster, and M.S. Barnes, Journal of Vacuum Science and Technology A, 11 (5), (1993) p 2487
1.3 P. Gadgil, D. Dane, and T.D. Mantei, Journal of Vacuum Science and Technology B, 11 (2), (1993) p 216
1.4 J. Hopwood, C.R, Guarnieri, S.J. Whitehair, and J.J. Cuomo, Journal of Vacuum Science and Technology A, 11 (1), (1993) p 152
1.5 H.J. Lee, I.D. Yang, and K.W. Whang, Plasma Sources and Science Technology, 5, (1996) p 383
1.6 J.A. Stittsworth and A.E. Wendt, Plasma Sources and Science and Technology, 5, (1196) p 429
1.7 R. Krimke, and H.M. Urbassek, Plasma Sources and Science and Technology, 5, (1996), p 389
1.8 M.A. Lieberman, and A.J. Lichtenberg, *Principles of plasma discharges and materials processing* (New York, Wiley, 1994)
1.9 F.F. Chen, and J.P. Change (New York, Kluwer/Plenum, 2003)
1.10 T. Kitajima, M. Izawa, R. Hashid, N. Nakono, And T. Makahe, Applied Physics Letters 69, (1996) p 758
1.11 S. Rauf and M.S. Kushner, IEEE Transactions on Plasma Science, 27, (1999), p 1329
1.12 T. Kitajima, Y Takeo, ZL Petrovic, and T. Makahe, Applied Physics Letters, 77, (2000), p 489
1.13 W. M. Manheimer, R. F. Fernsler, and M. Lampe, Plasma Sources Science and Technology, 9**,** (2000) p 370
1.14 S. G. Walton, C. Muratore, D. Leonhardt, R. F. Fernsler, D. D. Blackwell, and R. A. Meger, Surface & Coatings Technology, 186 (1/2), (2004) p 40
1.15 R. F. Fernsler, W. M. Manheimer, R.A. Meger, J. Mathew, D. P. Murphy, R. E. Pechacek, J. A. Gregor, Physics of Plasmas, 5 (5), (1998) p 2137
1.16 J. Mathew, R. F. Fernsler, R. A. Meger, J. A. Gregor, D. P. Murphy, R. E. Pechacek, and W. M. Manheimer, Physical Review Letters 77 (10), (1996) p 1982

Chapter 2:

2.1 D. Hegemann, H. Brunner, and C. Oehr, Nuclear Instruments and Methods in Physics Research B, 208, (2003) p 281
2.2 A. C. Fozza, J. E. Klemberg-Sapieha, and M. R. Wertheimer, Plasmas and Polymers, 4 (2/3), (1999) p 183
2.3 F. Truica-Marasescu, S. Guimond, and M. R. Wertheimer, Nuclear Instruments and Methods in Physics Research B 208, (2003) p 294
2.4 P. Favia, M. V. Stendardo, and R. d'Agostino, Plasmas Polymers, 1, (1996) p 91
2.5 M. Creatore, P. Favia, G. Tenuto, A. Valentini, and R. d'Agostino, Plasmas and Polymers, 5 (3/4), (2000) p 201

2.6 B. D. Beake, J. S. G. Ling, and G. J. Leggett, Journal of Materials Chemistry, 8, (1998) p 1735
2.7 K. S. Kim, C. M. Ryu, C. S. Park, F. S. Sur, and C. E. Park, Polymer, 44, (2003) p 6287
2.8 M. C. Coen, R. Lehmann, P. Groening, and L. Schlapbach, Applied Surface Science, 207, (2003) p 276
2.9 D. J. Barton, W. Bradley, K. J. Gibson, D. A. Steele, and R. D. Short, Journal of Physical Chemistry B, 104, (2000) p 7150
2.10 L. Ling, X. Hua, X.Li, G. S. Oehrlein, E. A. Hudson, P. Lazzeri, and M. Anderle, Journal of Vacuum Science and Technology B, 22 (6), (2004) p 2594
2.11 X. Hua, G. S. Oehrlein, P. Jiang, P. Lazzeri, E. Iacob, and M. Anderle, Submitted for Publication.
2.12 S. Lassig, and E. A. Hudson, Solid State Technology, 45 (10), (2002) p 47
2.13 L. Ling, X. Hua, L. Zheng, G. S. Oehrlein, E. A. Hudson, and P. Jiang, Submitted for Publication
2.14 R. F. Fernsler, W. M. Manheimer, R. A. Meger, J. Mathew, D. P. Murphy, R. E. Pechacek, J. A., Physics of Plasmas 5 (5), (1998) p 2137
2.15 W. M. Manheimer, R. F. Fernsler, and M. Lampe, Plasma Sources Science and Technology, 9**,** (2000) p 370
2.16 D. Leonhardt, S.G. Walton, D.D. Blackwell, W.E. Amatucci, D.P. Murphy, R.F. Fernsler, and R.A. Merger, Journal of Vacuum Science and Technology A, 19 (4), (2001) p 1367
2.17 S. G. Walton, D. Leonhardt, D. D. Blackwell, R. F. Fernsler, D. P. Murphy, and R. A. Meger, Journal of Vacuum Science and Technology A, 19 (4), (2001) p 1325
2.18 D. Leonhardt, C. Muratore, S. G. Walton, D. D. Blackwell, R. F. Fernsler, and R. A. Meger, Surface and Coatings Technology, (2004) p 682
2.19 D. Leonhardt, S. G. Walton, C. Muratore, R. F. Fernsler, and R. A. Meger, Journal of Vacuum Science and Technology A, 22 (6), (2004) p 2276
2.20 R.M.A. Azzam and N.M. Bashara, *Ellipsometry and polarized light*, (Amsterdam, North Holland 1977)
2.21 Tompkins *Spectroscopic Ellipsometry and reflectometry* (New York, John Wiley & Sons, 1999)
2.22 M. Schaepkens, T. E. F. M. Standaert, N. R. Rueger, P. G. M. Sebel, G. S. Oehrlein, and J. M. Cook, Journal of Vacuum Science and Technology A, 17 (1), (1999) p 26
2.23 G. S. Oehrlein, X. Hua, C. Stolz, and P. Jiang, Journal of Vacuum Science & Technology B, 24 (1), (2006) p 279
2.24 L. Ling, G. S. Oehrlein, E. A. Hudson, and P. Jiang, Submitted for Publication
2.25 X. Li, L. Ling, X. Hua, M. Fukasawa, G. S. Oehrlein, M. Barela, and H. M. Anderson, Journal of Vacuum Science and Technology A, 21 (1), (2003) p 284
2.26 A. A. Chambers, Solid State Technology, 48 (2), (2005) p 56
2.27 X. Li, X. Hua, L. Ling, G. S. Oehrlein, M. Barela, H. M. Anderson, Journal of Vacuum Science and Technology A, 20 (6), (2002) p 2052
2.28 D. Hyun-Ho, K. Jung-Hun, L. Seok-Hyun, and W. Ki-Woong, Journal of Vacuum Science and Technology A, 14 (5), (1996) p 2827

2.29 S. Wolf, and N. R. Tauber, *Silicon processing for the VLSI era*. (California, Lattice Press, 2000)
2.30 L. Zheng, L. Ling, X. Hua, G.S. Oehrlein, and E.A. Hudson, Journal of Vacuum Science & Technology A, 23 (4), (2005) p 634

Chapter 3:

3.1 E. Trabert, Canadian Journal of Physics, 8, (2002) p 1481
3.2 R.W. Odom, D.L Smith, J.H. Futrell, Journal of Physics B, 8 (8), (1975) p 1349
3.3 L. Ling, X. Hua, X.Li, G. S. Oehrlein, E. A. Hudson, P. Lazzeri, and M. Anderle, Journal of Vacuum Science and Technology B, 22 (6), (2004) p 2594
3.4 X. Hua, G. S. Oehrlein, P. Jiang, P. Lazzeri, E. Iacob, and M. Anderle, Submitted for Publication.
3.5 V. J. Law, M. Tewordt, D. C. Clary, and G. A. C. Jones, Journal of Vacuum Science and Technology B, 11, (1993) p 2262
3.6 S.G. Walton, D. Leonhardt, R.F. Fernsler, and R.A. Meger, Applied Physics Letters, 83 (4), (2003) p 626
3.7 S.G. Walton, D. Leonhardt, and RF Fernsler, IEEE Transactions on Plasma Science, 33 (2), (2005) p 838
3.8 S. G. Walton, D. Leonhardt, R.F. Fernsler, and R.A. Meger, Applied Physics Letters, 81 (6) (2002) p 987
3.9 Walton, S.G., Muratore, C., Leonhardt, D., Fernsler, R. F., Blackwell, D. D., and Meger, R. A., Surface and Coatings Technology, 186 (1/2), (2004) p 40
3.10 M. F. Doemling, B. Lin, N. R. Rueger, G. S. Oehrlein, R. A. Haring, and Y. H. Lee, Journal of Vacuum Science and Technology A, 18 (1), (2000) p 232
3.11 Giapis, K.P., T.A. Moore, and T.K. Minton, Journal of Vacuum Science and Technology A, 13 (3), (1995) p 959
3.12 T. Xianmin, C.A. Nichols, and D.M. Manos, Journal of Applied Physics, 86 (5), (1999) p 2419
3.13 T. J. Sommerer, and M. Kushner, Journal of Applied Physics, 70 (3), (1991) p 1240